Biochemical Analysis of *Thermotoga maritima* GH36 α-Galactosidase (*Tm*GalA) Confirms the Mechanistic Commonality of Clan GH-D Glycoside Hydrolases†

Donald A. Comfort,‡ Kirill S. Bobrov,§ Dina R. Ivanen,§ Konstantin A. Shabalin,§ James M. Harris,‡ Anna A. Kulminskaya,§ Harry Brumer,|| and Robert M. Kelly*,‡

Department of Chemical and Biomolecular Engineering, North Carolina State University, Raleigh, North Carolina 27695-7905, Petersburg Nuclear Physics Institute, Russian Academy of Science, Molecular and Radiation Biology Division, Gatchina, St. Petersburg 188300, Russia, and School of Biotechnology, Royal Institute of Technology, AlbaNova University Centre, Stockholm, Sweden

Received July 28, 2006; Revised Manuscript Received December 12, 2006

ABSTRACT: Organization of glycoside hydrolase (GH) families into clans expands the utility of information on catalytic mechanisms of member enzymes. This issue was examined for GH27 and GH36 through biochemical analysis of GH36 α-galactosidase from *Thermotoga maritima* (*Tm*GalA). Catalytic residues in *Tm*GalA were inferred through structural homology with GH27 members to facilitate design of site-directed mutants. Product analysis confirmed that the wild type (WT) acted with retention of anomeric stereochemistry, analogous to GH27 enzymes. Conserved acidic residues were confirmed through kinetic analysis of D327G and D387G mutant enzymes, azide rescue, and determination of azide rescue products. Mutation of Asp327 to Gly resulted in a mutant that had a 200−800-fold lower catalytic rate on aryl galactosides relative to the WT enzyme. Azide rescue experiments using the D327G enzyme showed a 30-fold higher catalytic rate compared to without azide. Addition of azide to the reaction resulted in formation of azide β-D-galactopyranoside, confirming Asp327 as the nucleophilic residue. The Asp387Gly mutation was 1500-fold catalytically slower than the WT enzyme on *p*-nitrophenyl α-D-galactopyranoside. Analysis at different pH values produced a bell-shaped curve of the WT enzyme, but D387G exhibited higher activity with increasing pH. Catalyzed reactions with the D387G mutant in the presence of azide resulted in formation of azide α-D-galactopryanoside as the product of a retaining mechanism. These results confirm that Asp387 is the acid/base residue of *Tm*GalA. Furthermore, they show that the biochemical characteristics of GH36 *Tm*GalA are closely related to GH27 enzymes, confirming the mechanistic commonality of clan GH-D members.

α-D-Galactosidases (EC 3.2.1.22) are exo-acting glycoside hydrolases that cleave α-linked galactose residues from carbohydrates commonly found in legumes and seeds, such as melibiose, raffinose, stachyose, and gluco- or galactomannans (*1*). α-Galactosidases and related enzymes are of interest for both physiological and biotechnological applications. In humans, Fabry's disease is an X-linked lysosomal storage disorder, in which glycosphingolipids form with terminal α-galactosidase sugars. Inactive mutant α-galactosidase enzymes cannot remove these terminal galactose sugars, thus preventing degradation of the glycosphingolipids. Enzyme replacement therapy has been shown to successfully treat the disease (*2*, *3*). Similarly, deficiencies in α-*N*-acetylgalactosaminidases cause a related genetic lysosomal storage disorder, Schindler disease (*4*). α-Galactosidases have been used for biotechnological purposes, including pretreatment of animal feed to hydrolyze nonmetabolizable sugars, thereby increasing the nutritive value (*5*), degradation of raffinose to improve the crystallization of sucrose (*6*), processing of soy molasses and soybean milk (*7*), improvement of the viscosity and gelling properties of galactomannan (*8*, *9*), stimulation of oil/gas wells through hydrolysis of the propant matrix (*10*), and conversion of B-type blood antigens to produce type O blood (*11*−*14*). Because of their medical and technological importance, a number of α-galactosidases from eukaryotic and microbial sources have been studied (*15*−*19*).

α-Galactosidases have been classified by substrate specificity (*8*) and by sequence similarity using hydrophobic cluster analysis (*20*). With respect to substrate specificity, group I α-galactosidases hydrolyze oligosaccharides, such as melibiose, stachyose, raffinose, and verbacose; group II α-galactosidases are active on polysaccharide substrates, such as galactomannan and glucomannan. In the carbohydrate-active enzyme family classification scheme, which groups

† R.M.K. acknowledges support from the Biotechnology Program of the U.S. National Science Foundation and Energy Biosciences Program of the U.S. Department of Energy. A.A.K. and co-workers acknowledge the Program for Basic Research in Molecular and Cell Biology from the Presidium of the Russian Academy of Sciences (PRAS) and the Scientific Program of the St. Petersburg Scientific Center. H.B. thanks the Swedish Science Council (Vetenskapsrådet) for a Special Council Research Position (Rådsforskare) and the Swedish Foundation for Strategic Research (SSF) for partial funding of this research.

* Address correspondence to this author. Phone: 919-515-6396. Fax: 919-515-3465. E-mail: rmkelly@eos.ncsu.edu.

‡ North Carolina State University.

§ Petersburg Nuclear Physics Institute, Russian Academy of Science.

|| AlbaNova University Centre.

10.1021/bi061521n CCC: $37.00 © 2007 American Chemical Society
Published on Web 02/27/2007

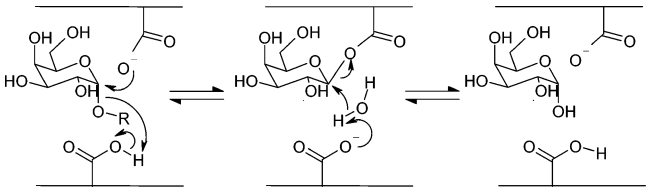

FIGURE 1: Retaining glycosidase mechanism in which a double displacement mechanism generates a product with the same anomeric configuration as the initial substrate.

glycoside hydrolases (GH)[1] on the basis of amino acid sequence and structural similarities [http://afmb.cnrs-mrs.fr/CAZY/index.html (*20*−*22*)], α-galactosidases are found in GH4, GH27, GH36, and GH57. α-Galactosidases from eukaryotic organisms are predominantly grouped into family GH27, whereas those from microbial sources are primarily grouped into families GH4, GH36, and GH57. Of these, families GH27 and GH36 are thought to share a common ancestral gene, forming the glycoside hydrolase clan (GH-D) with a common triosephosphate isomerase (TIM) barrel structure (*20*, *23*).

Seven apo and ligand-complex three-dimensional structures for GH27 enzymes from four organisms have been determined, including an *N*-acetyl-α-galactosaminidase from *Gallus gallus* (chicken) (*24*), an α-galactosidase A from *Homo sapiens* (human) (*25*), an α-galactosidase from the fungus *Hypocrea jecorina* (née *Trichoderma reesei*) (*26*, *27*), and an α-galactosidase from *Oryza sativa* (rice) (*28*). Early work on the main α-galactosidase from the white-rot fungus *Phanerochaete chrysosporium* (*29*) established that enzymes in GH27 act through a double-displacement mechanism involving retention of the stereochemistry of the anomeric center (Figure 1) (*30*). Specific mechanism-based inactivation, coupled with mass spectrometry, was subsequently used to identify the conserved catalytic nucleophile in this family for both the *P. chrysosporium* (*31*) and the *Coffea arabica* (coffee) (*32*) α-galactosidases. The analysis of three-dimensional enzyme−product complexes later facilitated identification of the conserved catalytic general acid/base residue (*24*−*26*, *28*, *33*).

In contrast to GH27 members, the molecular details governing catalysis by GH36 enzymes are less clear. Members of GH36 are particularly interesting enzymes with respect to their potential for carbohydrate synthesis through protein engineering, since both hydrolytic (α-galactosidase and *N*-acetyl-α-galactosaminidase) and transglycosylation activities (raffinose and stachyose synthase) are represented in this group. Previously, global protein sequence analysis established the relationship of GH27 and GH36 in clan GH-D (*22*), thus implying a conserved overall $(\beta/\alpha)_8$ tertiary structure and retaining catalytic mechanism. However, sequence similarity within clan GH-D was too low to accurately predict the location of key amino acids. Structural information on the GH36 α-galactosidase from *Thermotoga maritima* (*Tm*GalA) enzyme has recently been deposited (*34*), facilitating efforts to compare catalytic mechanisms of GH27 and GH36. As such, site-directed mutagenesis and detailed kinetic analysis of *Tm*GalA have led to identification of the key catalytic and active site residues in GH36, suggesting that a common mechanism governs enzymes in clan GH-D.

EXPERIMENTAL PROCEDURES

Materials and General Procedures. Chemicals, growth media, and buffer reagents were obtained from Fisher Scientific (Hampton, NH) and Sigma-Aldrich (St. Louis, MO). All protein structure figures were produced using PyMOL v0.98 or v0.99, available at URL http://pymol.sourceforge.net/.

Synthesis of α*-Galactosides.* All *o*-nitrophenyl and *p*-nitrophenyl (Gal-PNP) glycosides were purchased from Sigma-Aldrich (St. Louis, MO). 4-Bromophenyl, 3,4-dimethylphenyl, 4-methoxyphenyl, phenyl, and *m*-nitrophenyl α-D-galactopyranosides were synthesized from galactose by acetylation, fusion of the acetates with corresponding phenol and anhydrous zinc chloride as described (*35*), and Zemplén deacetylation. 2,4-Dinitrophenyl, 2,5-dinitrophenyl, and 2-naphthyl α-D-galactopyranosides were synthesized from tetra-*O*-acetyl α-D-galactopyranosyl chloride (*36*), and sodium salts of corresponding phenols in HMPA were prepared as described elsewhere (*37*, *38*). Dinitrophenyl derivatives were deacetylated at 4 °C in anhydrous methanol saturated with HCl (*29*). Deprotection of 2-naphthyl α-D-galactoside was achieved by the Zemplén procedure. All products were obtained in crystalline form and characterized by ^{1}H NMR analysis (Supporting Information). These data were consistent with the expected structure and literature data (when available) in each case.

Cloning, Mutagenesis, Protein Expression, and Protein Purification. Recombinant *Escherichia coli* strains were grown in Luria broth containing 50 mg/L kanamycin. The α-galactosidase gene (*galA*) from *T. maritima* MSB8 (ORF TM1192) was amplified from genomic DNA by PCR using primers (direct, 5′-CGCGCCATGGAAATATTCGGAAA-GACCTTCAG-3′; reverse, 5′-GCGCGAATTCTACCT-GAGTTCCATCATT-3′), which introduced *Nco*I and *Eco*RI restriction sites (underlined) and, in the process, mutated the first codon of the gene from GTG to ATG. The PCR fragment was inserted into pET24d (Novagen, San Diego, CA) and sequenced to verify cloning. Mutant clones were generated using the QuikChange site-directed mutagenesis kit (Stratagene, La Jolla, CA) with the corresponding primer listed in Table 1 and its complement. Recombinant α-galactosidase (*Tm*GalA) and its derived mutants were expressed in *E. coli* BL-21(DE3) from cultures grown overnight, and the proteins were purified as previously described (*39*). In the case of the mutants, new column matrix was used for each mutant. Protein concentrations were determined using the Bio-Rad protein assay (Bio-Rad, Hercules, CA) with bovine serum albumin as standard.

NMR and MS Analyses of Reaction Products. All ^{1}H spectra were recorded with an AMX-500 Bruker spectrophotometer. Prior to analysis by NMR, *Tm*GalA wild type (WT), D327G and D387G mutants, buffer materials, and substrates were freeze-dried twice with D_2O. The ^{1}H NMR measurements were performed in 50 mM sodium acetate (pH 5.0) buffer with acetone used as an internal standard (δ ^{1}H 2.23). Product formation and stereochemistry of Gal-PNP hydrolysis were determined using ^{1}H NMR spectroscopy,

[1] Abbreviations: Gal-PNP, *p*-nitrophenyl α-D-galactopyranoside; GH, glycosyl hydrolase; N_3αGal*p*, azide α-D-galactopyranoside; $N_3\beta$Gal*p*, azide β-D-galactopyranoside; *Tm*GalA, *Thermotoga maritima* α-galactosidase; WT, wild-type enzyme.

Table 1: Primer Pairs for *T. maritima* α-Galactosidase Site-Directed Mutants (Complementary Primer Not Shown)

mutation	primer
D103A	GG AAC CTC CAG AGC GCC TAT TTC GTG GCT GAA GAA GG
D220A	C GAG GTC TTC CAG ATA GCC GAC GCC TAC GAA AAG GAC
D220G	C GAG GTC TTC CAG ATA GGT GAC GCC TAC GAA AAG GAC
D220A	G GTC TTC CAG ATA GAC GCC GCC TAC GAA AAG GAC ATA GG
D229A	C TAC GAA AAG GAC ATA GGT GCC TGG CTC GTG ACA AGA GG
D275A	GTA TTC AAC GAA CAT CCG GCC TGG GTA GTG AAG GAA AAC GG
D299A	G ATA TAC GCC CTC GCT CTT TCG AAA GAT GAG GTT CTG AAC TG
D327A	C TAC AGG TAC TTC AAG ATC GCC TTT CTC TTC GCG GGT GC
D327G	C TAC AGG TAC TTC AAG ATC GGC TTT CTC TTC GCG GGT GC
D387G	GG ATG AGG ATA GGA CCT GGT ACT GCG CCG TTC TG

by on-line detection of the products formed. Galactose concentrations at different time intervals during the reaction were determined using specific chemical shifts: α-galactose, $\delta = 5.26$; β-galactose, $\delta = 4.58$. NMR analysis of azide rescue experiments for D327G and D387G mutants was carried out as follows. ^{1}H NMR spectra were collected for hydrolysis of 1 mM Gal-PNP with 0.02 unit of each enzyme in 50 mM sodium phosphate, pH 6.5, with 100 mM NaN_3. Spectra were recorded every 15 min until the reaction was completed.

Products of the azide rescue reaction of D327G enzyme were separated using a Spherisorb C8 column (250 × 4.6 mm; Supelco Inc.). Mass spectrometric analysis of these products was performed with a Q-Tof 2 mass spectrometer fitted with a nanoflow ion source (Waters Corp., Micromass MS Technologies, Manchester, U.K.) as described (*40*).

Reaction Kinetics and Biochemical Characterization. Kinetic studies of *Tm*GalA WT and D327G were performed on a Jasco V-560 UV−vis spectrometer, equipped with a circulating water bath, using 1 cm path length quartz cuvettes. The buffer employed for all kinetic experiments with WT enzyme was 50 mM sodium acetate (pH 5.0), containing 0.5 mg/mL BSA in the case of the WT enzyme. Extinction coefficients for phenols were determined by measuring the absorbance of each compound in the same buffer at 37 °C. This temperature was chosen to minimize spontaneous hydrolysis of the substrates. The wavelength monitored and molar extinction coefficients used for each substrate were as follows ($\Delta\epsilon$, mM^{-1} cm^{-1}): 2′,4′-dinitrophenyl, 440 nm, 8.48; 2′,5′-dinitrophenyl, 440 nm, 3.44; 4′-nitrophenyl, 400 nm, 7.61; 2′-nitrophenyl, 265 nm, 2.15; 4′-methylumbelliferyl, 355 nm, 2.87; 3′-nitrophenyl, 380 nm, 0,49; 4′-bromophenyl, 289 nm, 0.94; β-naphthyl, 330 nm, 1.47; 4-*O*-methylphenyl, 285 nm, 1.93; 3′,4′-dimethylphenyl, 285 nm, 1.29; phenyl, 277 nm, 0.863.

Substrate hydrolysis was initiated with the addition of an appropriate aliquot of enzyme (0.47 μg of WT protein and 39−62 μg of D327G mutant enzyme); the initial rate of phenolate release was monitored at 37 °C at an appropriate wavelength relative to a reference cuvette containing no enzyme. The rate of enzyme-catalyzed hydrolysis was determined by varying substrate concentrations (typically 10−12 points) ranging from 0.5 × 5 to 10K_m, when possible. The kinetic parameters were estimated by direct fit of the data to the Michaelis−Menten equation using the program Origin 7.5 (OriginLab Corp., Northampton, MA). Logarithmic plots of kinetic parameters (k_{cat} and k_{cat}/K_m) were fitted by linear regression with the leaving group pK_a values. The Brønsted coefficients, β_{lg}, were calculated from the slopes of these plots.

Azide rescue reactions using the D327G mutant were performed in 50 mM sodium acetate buffer with 0−400 mM sodium azide, measuring hydrolysis of 2.5 mM Gal-PNP at 37 °C for 20 min. Reactions were stopped by the addition of 10% sodium carbonate. Addition of azide resulted in an increase of pH from 5.0 to 6.2 for 400 mM NaN_3. Hydrolysis was monitored using the Jasco spectrometer as described above.

Kinetic studies on the D387G mutant were conducted at 37 °C using Gal-PNP as substrate on a Perkin-Elmer Lambda Bio 20 spectrophotometer (Wellesley, MA), heated by a Perkin-Elmer PTP-1 Peltier system. Experiments were run in 200 mM sodium citrate buffer (pH 5.0). The activity assay was modified to increase sensitivity by changing to an end point assay, which was stopped after 5 min by addition of 1 M Na_2CO_3. This changed the extinction coefficient to 18 mM^{-1} cm^{-1}. Michaelis−Menten kinetic parameters were calculated by least-squares regression in Excel (Microsoft, Redmond, WA). The influence of external nucleophiles on WT and D387G was studied using Gal-PNP at concentrations from 12 μM to 2 mM. Azide rescue experiments were conducted in the presence of 2 M sodium azide with 200 mM sodium citrate, pH 5.0 (after addition of azide). Formate rescue experiments were conducted in 2 M sodium formate buffer (pH 5.0).

The pH dependence of enzymatic hydrolysis was investigated by determining k_{cat} and K_m values for a series of pH values between 2.5 and 8.5. Hydrolysis of Gal-PNP at 37 °C was continuously monitored at 400 nm. Only pHs for which the enzyme was stable for at least 25 min were used. All buffers [citrate−phosphate buffer solutions (pH 2.8−7.5); glycine buffers (pH 8.0−10.5)] were at a final concentration 50 mM and contained 0.05 M NaCl. Reaction mixtures (total volume of 600 μL) were prewarmed until the reaction was initiated by the addition of 0.4 μg of WT, approximately 60 mg of D327G, or 147 mg of D387G. Kinetic parameters determined at each pH were then fitted with a function describing a bell-shaped pH profile (eq 1a,b) using Origin 7.5, yielding the apparent pK_a of the ionizable groups.

$$k_{cat} = \frac{(k_{cat})_{max} \times 10^{pH-pK_{a1}}}{10^{2pH-pK_{a1}-pK_{a2}} + 10^{pH-pK_{a1}} + 1} \quad (1a)$$

$$k_{cat}/K_m = \frac{(k_{cat}/K_m)_{max} \times 10^{pH-pK_{a1}}}{10^{2pH-pK_{a1}-pK_{a2}} + 10^{pH-pK_{a1}} + 1} \quad (1b)$$

Differential Scanning Microcalorimetry. Purified proteins were dialyzed overnight against 2 L of filtered 50 mM

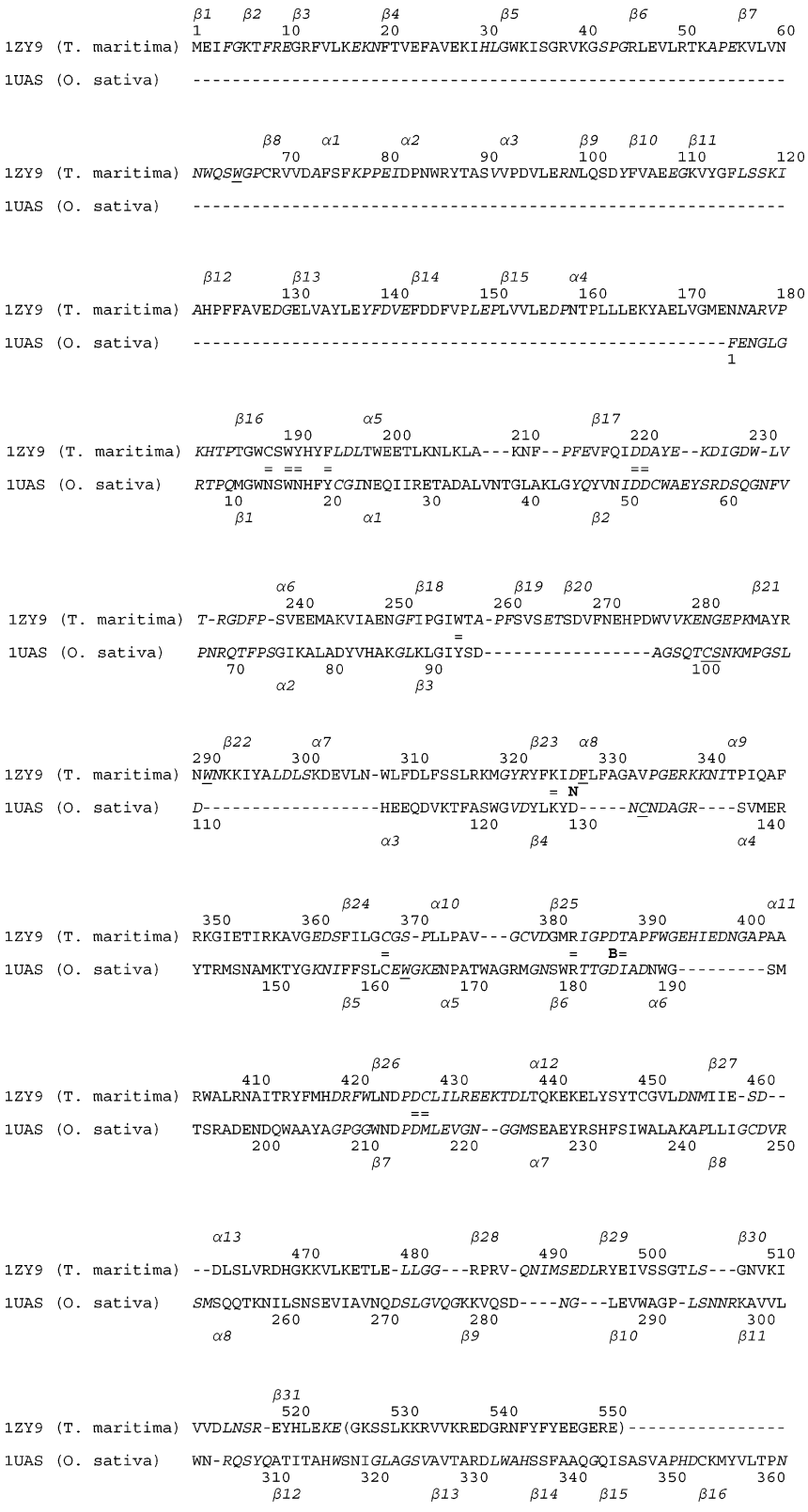

FIGURE 2: Structure-based protein sequence alignment of *Tm*GalA (PDB 1ZY9, UniProt O33835) and *O. sativa* α-galactosidase (PDB 1UAS, UniProt Q9FXT4). The respective PDB file residue numbering systems are used. Secondary structural elements extracted by PyMOL from the PDB data are highlighted. Secondary structure element numbering for 1UAS is from Fujimoto et al. (*28*). Residues in loop regions are shown in italics. Spatially equivalent residues in the enzyme active sites are denoted with "=". The following underlined residues are also approximately equivalent in the active site: 1ZY9 W65 = 1UAS W164; 1ZY9 F328 and W291 = 1UAS C101−C132 disulfide and S102. The catalytic nucleophile residue in each enzyme is marked with an N and the general acid/base residue with a B. Residues 526−551, in parentheses, were not observed in the crystal structure of *Tm*GalA.

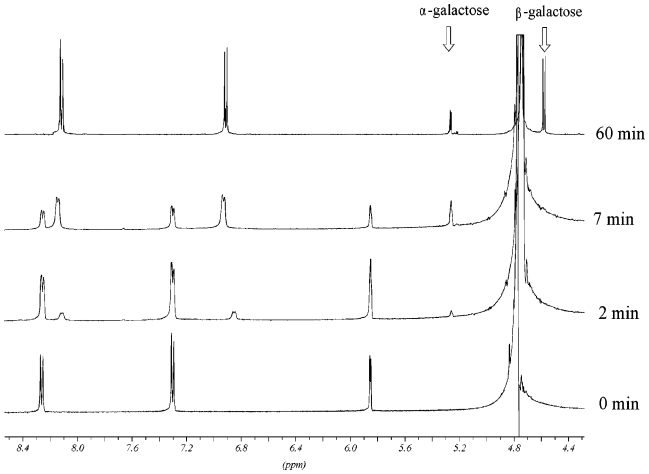

FIGURE 3: ^{1}H NMR analysis of the stereoselectivity for the WT *Tm*GalA catalyzed reaction.

sodium phosphate, pH 7.2, with 150 mM NaCl. Samples of 1.5−3.0 mg/mL protein were run on an N-DSC (Calorimetry Sciences Corp., Lindon, UT) from 25 to 125 °C at 0.5 °C/s. Results were analyzed using CpCalc 2.0 (Calorimetry Sciences Corp.), and the maximum excess heat capacity was used as the melting temperature of the proteins.

RESULTS

Substrate Specificity of TmGalA on Glycosides. A series of 4-nitrophenyl glycosides and natural galactosylated substrates were used to determine the substrate specificity. Using accepted nomenclature (*41*), the glycone occupies the −1 subsite in the enzymatic active site pocket, while the departing group occupies the +1 subsite. As there was no detectable enzymatic activity on xylo-, fuco-, manno-, or glucopyranosides (data not shown), it appears that *Tm*GalA prefers substrates with galactopyranoside as the glycone.

Site-Directed Mutagenesis of TmGalA Active Site Residues. The primary sequence of *Tm*GalA is shown in Figure 2. Conserved acidic amino acid residues in GH36 were identified by sequence alignments with other GH36 α-galactosidases (*42*), and alanine mutants were generated for the conserved residues D103, D220, D221, D229, D275, D299, D327, and D387. Site-directed mutations, D220A, D327A, and D387A, generated products that exhibited less than 1% of the wild-type (WT) enzyme activity on Gal-PNP in sodium acetate at 80 °C, implicating their role in catalysis. These residues were mutated to glycine for further analysis.

Stereochemical Course of the Hydrolytic Reaction. ^{1}H NMR provides a direct method for determining a stereochemical outcome of the glycoside hydrolysis. Chemical shifts and coupling constants of the anomeric protons in α- and β-glycosides, as well as in the product hemiacetals, are distinct and readily observed. Figure 3 shows the kinetics of the formation of α- and β-anomers of galactose in the hydrolysis of Gal-PNP. The α-anomer was initially formed in the presence of the WT enzyme and accumulated in amounts sufficient for detection, followed by a noticeable amount of β-anomer, which appeared due to mutarotation. Mutarotation proceeded until the normal anomer ratio of 30% α- and 70% β-galactopyranose was established (60 min after the reaction was stopped). The data unequivocally demonstrate that enzymatic hydrolysis proceeds with the retention of the anomeric configuration, presumably as a result of a double displacement reaction (*43*). The stereochemical outcome of the hydrolysis of Gal-PNP catalyzed by D387G was monitored by NMR. An accumulation of α-D-galactose as an initial reaction product was observed, followed by the appearance of a small amount of β-anomer arising due to mutarotation. This fact indicates the D387G mutant to be a retaining glycoside hydrolase similar to the WT.

Analysis of Structural Features of TmGalA with Respect to the Biocatalytic Mechanism. The tertiary structure of *Tm*GalA consists of three domains (Figure 4): an N-terminal β-supersandwich domain (residues 1−179; see Figure 2 for primary sequence), a core $(\beta/\alpha)_8$ barrel (residues 180−482), and a C-terminal antiparallel β-sheet domain (residues 483−525) (*34*). As expected, based on common clanship in GH-D (*22*) (URL: http://afmb.cnrs-mrs.fr/CAZY/), *Tm*GalA from GH36 shares a homologous $(\beta/\alpha)_8$-barrel catalytic domain with all of the known three-dimensional structures of GH27 enzymes (Figure 5). DaliLite (*44*) was used for pairwise comparison of *Tm*GalA with representative structures from *H. sapiens* α-galactosidase A (PDB 1r46) (*25*), *H. jecorina* (née *T. reesei*) α-galactosidase (PDB 1SZN) (*26*), *O. sativa* α-galactosidase (PDB 1UAS) (*28*), and *G. gallus N*-acetyl-α-galactosaminidase (PDB 1KTB) (*24*). As shown in Table 2, comparison of the complete structures indicated modest structural overlap, as judged by the rmsd values of the C^α atoms, despite very low sequence similarity. Both the rmsd values and *Z*-scores were slightly improved when only the corresponding $(\beta/\alpha)_8$-barrel domains were compared, which indicates minimal structural homology of the C-terminal β-sheet domain observed in GH27 enzymes. Indeed, there is an apparent lack of overlap of the C^α trace of *Tm*GalA

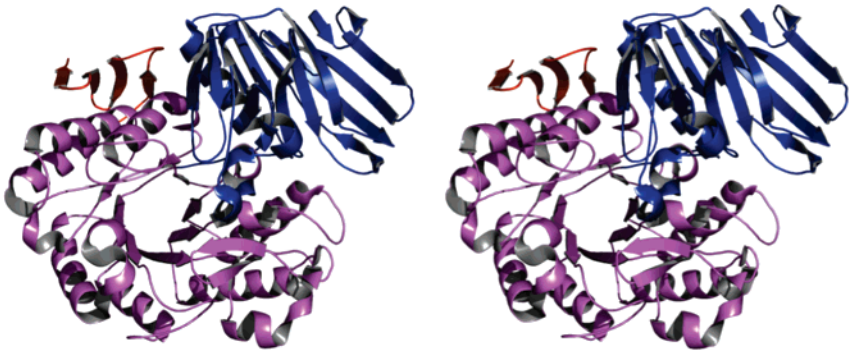

FIGURE 4: Wall-eyed stereo overview of the *Tm*GalA tertiary structure and secondary structural elements. The N-terminal, $(\beta/\alpha)_8$-barrel, and C-terminal domains are colored in blue, violet, and red, respectively.

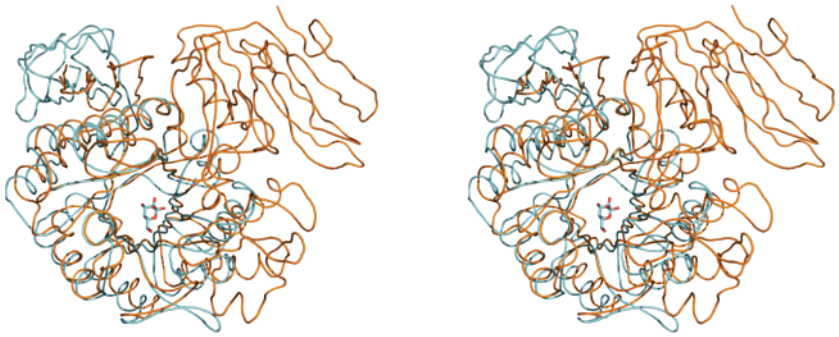

FIGURE 5: Superposition of the C^{α} traces of GH36 *Tm*GalA (PDB 1ZY9, orange) and the GH27 *O. sativa* α-galactosidase (PDB 1UAS, cyan). The wall-eyed stereoview is down the axis of the $(\beta/\alpha)_8$-barrel domain; the perspective is identical to that in Figure 4. Galactose, observed as an equilibrium mixture of α- and β-anomers in the *O. sativa* structure (*28*), highlights the position of the enzyme active sites.

Table 2: Structural Similarity between *Tm*GalA (PDB Code 1ZY9) and GH27 Members[a]

GH27 enzyme	PDB code	input residues (PDB numbering)	*Z*-score	aligned C^{α} residues	rmsd (Å)	sequence identity (%)
H. sapiens α-galactosidase A	1R46 (chain A)	32−421 (complete)	19.7	240	2.9	14
		32−328 [$(\alpha/\beta)_8$ domain]	22.2	236	2.7	14
H. jecorina (née *T. reesei*) α-galactosidase	1SZN	1−417 (complete)	18.6	276	2.9	18
		1−319 [$(\alpha/\beta)_8$ domain]	22.5	235	2.6	20
O. sativa α-galactosidase	1UAS	1−362 (complete)	21.1	268	2.8	16
		1−278 [$(\alpha/\beta)_8$ domain]	23.4	233	2.6	18
G. gallus N-acetyl-α-galactosaminidase	1KTB	1−388 (complete)	19.6	271	2.9	15
		1−298 [$(\alpha/\beta)_8$ domain]	22.5	236	2.7	15

[a] Pairwise structural alignments were performed using DaliLite (*44*) (accessed at the European Bioinformatics Institute at URL http://www.ebi.ac.uk/dali/index.html. For alignment with other complete sequences, *Tm*GalA residues 1−525 (PDB numbering) were used as input. For alignment of $(\alpha/\beta)_8$ domains, *Tm*GalA residues 180−479 were used as input.

with that of the representative *O. sativa* α-galactosidase (Figure 5). Furthermore, nearly 30 residues at the C-terminus of *Tm*GalA were not observed crystallographically. No binding nor catalytic function has been previously ascribed to this domain in GH27.

The three-dimensional structures of the GH27 enzymes have been rigorously compared and show little variation with regard to tertiary structure (*24*−*26*, *28*). The $(\beta/\alpha)_8$ and C-terminal domains are clearly superimposable (*45*), while only the *T. reesei* α-galactosidase (PDB 1SZN) is peculiar with regard to two loop extensions on the $(\beta/\alpha)_8$ barrel (*26*). Due to the high structural similarity within GH27, we selected the *O. sativa* α-galactosidase (PDB 1UAS) as an illustrative structure for further comparison with *Tm*GalA of GH36 (Figure 5). Manual analysis of the superimposed *O. sativa* and *T. maritima* enzymes was used to derive the primary sequence alignment shown in Figure 2.

The N-terminal β-supersandwich has no homologous structure in family GH27 enzymes of clan GH-D (cf. Figures 2 and 5) but bears the highest structural similarity to chain D of bovine lysosomal α-mannosidase (bLAM, PDB 1O7D) from GH38 (*46*). Analysis using Dali v.2.0 (*47*), via the Dali server (URL: www.ebi.ac.uk/dali/), indicated that residues 1−179 of *Tm*GalA (PDB 1ZY9) align with PDB 1O7D:chain D with a *Z*-value of 8.0, an rmsd value of 3.7 Å, and a sequence identity of 11% over 138 of 269 residues. The Secondary Structure Matching (SSM) server (*48*) (URL: www.ebi.ac.uk/msd-srv/ssm/) similarly returned PDB 1O7D: chain D as the top hit, with an rmsd value of 2.8 Å for 132 aligned residues with 11 aligned secondary structural elements, 14 gaps, and 11% sequence identity. A superposition of the N-terminal domain of *Tm*GalA with the D peptide of bLAM based on the SSM output is shown in Figure 6. Interestingly, this domain contributes a key substrate-binding residue (W65) to the active site of *Tm*GalA, which replaces the homologous W164 (Figures 2 and 7).

Indeed, a high degree of homology was observed between the active sites of *Tm*GalA and the *O. sativa* α-galactosidase (Figure 7). Galactose, observed as an equilibrium mixture of α- and β-anomers in the *O. sativa* structure, provides a convenient point of reference for the identification of the corresponding catalytic and substrate-binding residues in the active site of *Tm*GalA, which are summarized in Figure 2. Many active site residues are identical between the two enzymes, or are conservative substitutions, while in some cases more radical replacements are observed. As mentioned above, *Tm*W65, which is found on the loop joining β7 and β8 of the N-terminal β-supersandwich, replaces *Os*W164 from the loop joining β5 and α5 of the $(\beta/\alpha)_8$ barrel. Likewise, the side chains of F328 and W291 in *Tm*GalA approximately assume the position occupied by the S102 and C101-C132 cystine residue in the *O. sativa* enzyme. The *Tm*W191-*Os*D17 replacement is similarly nonconservative, but is compensated for, in part, by the *Tm*C428-*Os*M217 substitution. The conserved catalytic nucleophile and general acid/base residues in GH27, represented by D130 and D185 in the *O. sativa* α-galactosidase, are clearly observed to have structural homologues in *Tm*GalA, namely, D327 and D387, respectively.

Thermal Denaturation of WT and TmGalA Mutants. The melting behavior of the WT and mutant enzymes revealed that D327G had a nearly identical T_{melt} to the WT (89.8 °C), whereas D220G and D387G melted close to 83 °C (Table 3). Despite the role of D387 in catalysis, mutation of this

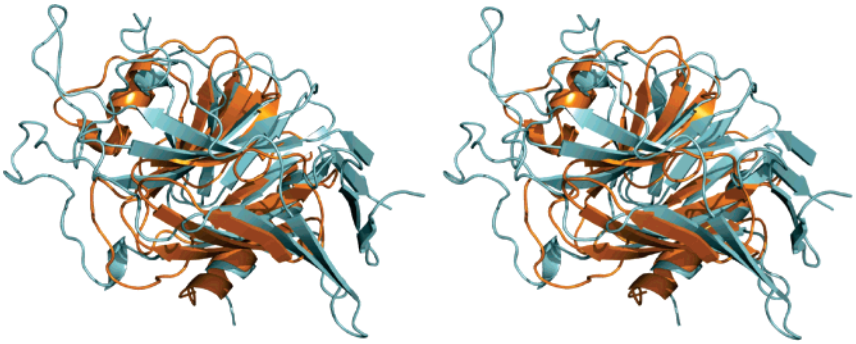

FIGURE 6: Wall-eyed stereoview of the N-terminal domain (residues 1−179) of GH36 *Tm*GalA (PDB 1ZY9, orange) superimposed on peptide D of GH38 bovine lysosomal α-mannosidase (PDB 1O7D:chain D, cyan).

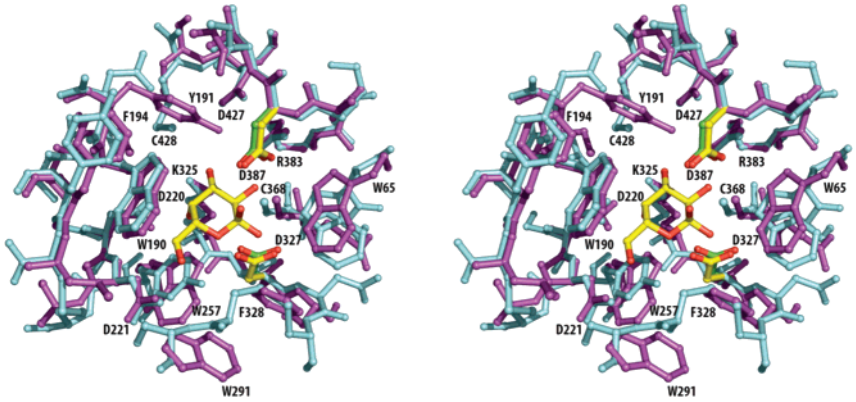

FIGURE 7: Superposition of the active sites of GH36 *Tm*GalA (PDB 1ZY9, violet) and the GH27 *O. sativa* α-galactosidase (PDB 1UAS, cyan). Bound galactose, as well as the catalytic nucleophile (D130) and general acid/base (D185) residues, in the *O. sativa* structure is shown in yellow/red. The corresponding nucleophile and acid/base residues in the *Tm*GalA structure are D327 and D387, respectively (green/red). Residue numbering is shown for *Tm*GalA, following the numbering scheme in PDB 1ZY9.

Table 3: Thermal Denaturation of *Tm*GalA and Mutants

enzyme	melting temp (°C)
wild type	89.8
D220G	82.8
D327G	89.0
D387G	83.3

amino acid adversely affected the stability of the enzyme. Residue D220 is positioned near the active site pocket, and the mutation affected the enzymatic activity of the enzyme as well as the stability of the protein, possibly due to elimination of a salt bridge with K325.

pH Dependence of Glycoside Hydrolysis. WT hydrolysis of Gal-PNP followed a standard bell-shaped (Figure 8), pH dependence, as expected for glycosidases, presumed to result from the ionization of the two active site carboxylic acids (*49*). The pH curve for D327G was similar in shape to the WT curve, but with a slight increase in pH optimum for k_{cat} (Figure 8a). The D387G pH profile, however, showed increasing activity with increasing pH (Figure 8). This has also been shown for the β-xylosidase from *Bacillus stearothermophilus* (*49*) and the α-arabinosidase from *Geobacills stearothermophilus* (*50*) acid/base mutants. In the case of the D387G, at high pH values there is no reduction in activity due to elimination of the acid/base residue. D220G exhibited a standard bell-shaped pH profile with a pH optimum of about 5.0 (results not shown) but with reduced activity relative to the WT protein.

Catalytic Properties of D327G and D387G Mutants. A series of aryl α-galactosides was used to examine the kinetic parameters of WT and D327G enzymes (Table 4). For both the WT and the D327G mutant, Brønsted plots and coefficients (see Figure 9) indicated that there was a linear, monotonic relationship between aryl α-D-galactopyranosides and the leaving group (WT $\beta_{1g} = -0.05$ for both k_{cat} and k_{cat}/K_m; D327G $\beta_{1g} = -0.15$ and -0.11 for k_{cat} and k_{cat}/K_m, respectively). The catalytic rates of the WT enzyme were 200−800-fold greater than the rates for the D327G mutant, while K_m values were of the same order of magnitude. This resulted in a lower (300−1700-fold) catalytic efficiency for the mutant relative to the WT. The reaction rates for WT and D387G enzymes for hydrolysis of Gal-PNP showed that the WT had approximately a 1500-fold higher catalytic rate than did D387G and a 1000-fold higher catalytic efficiency (Table 5).

External nucleophile rescue methodology was attempted using azide for WT, D327G, and D387G enzymes. No increase in the catalytic rate or efficiency was observed for the WT in the presence of either azide or formate. However, as expected, a noticeable restoration of hydrolytic activity for the nucleophilic mutant (D327G) was observed when azide was added into the reaction with Gal-PNP. The increase in rate was about 30-fold and clearly dependent on exogenous nucleophile concentration (Figure 10). Even a small concentration of azide (40 mM) restored the activity of this mutant up to 10-fold. Components of the reaction mixture with the D327G mutant after the hydrolysis of Gal-PNP in

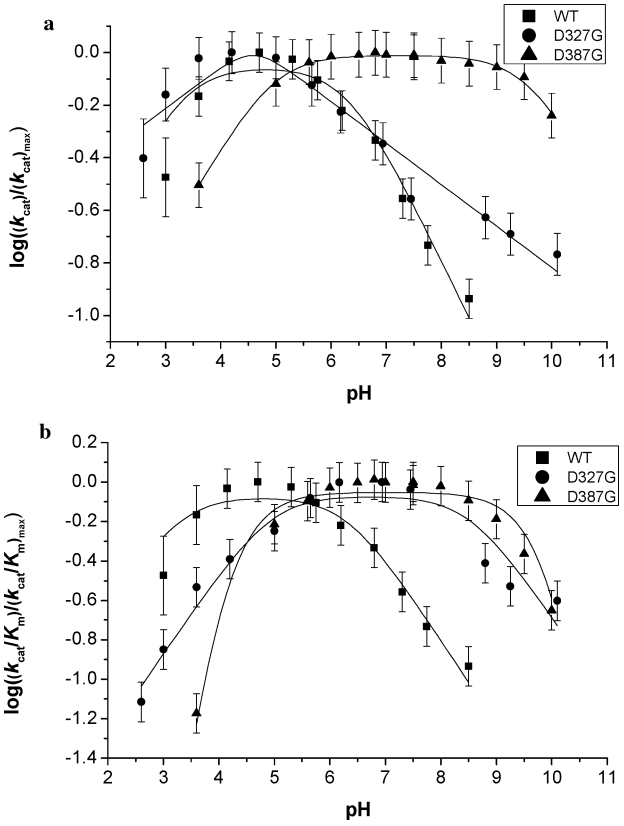

FIGURE 8: pH dependence of kinetic parameters. (a) log[$(k_{cat}/K_m)/(k_{cat}/K_m)_{max}$] of wild-type, D327G, and D387G enzymes versus pH. Calculated values for pK_{a1} and pK_{a2}: 3.3 and 6.29 (WT); 4.92 and 8.57 (D327G); 4.83 and 9.34 (D387G). (b) log[$(k_{cat})/(k_{cat})_{max}$] of wild-type, D327G, and D387G enzymes versus pH. Calculated values for pK_{a1} and pK_{a2}: 3.3 and 6.29 (WT); 2.73 and 6.46 (D327G); 4.95 and 9.51 (D387G). Lines were fit to experimental data using eq 1a,b (see Experimental Procedures).

Table 4: Steady-State Kinetic Parameters for the Hydrolysis of Aryl α-Galactosides by *Tm*GalA WT and D327G Enzymes

aglycon	pK_a	enzyme	k_{cat} (s^{-1})[a]	K_m (mM)	k_{cat}/K_m (s^{-1} mM^{-1})
2,4-dintrophenyl	3.96	WT	12.23	0.037	330.5
		D327G	0.085	0.135	0.630
2,5-dintrophenyl	5.15	WT	11.20	0.143	78.3
		D327G	0.042	0.243	0.173
4-nitrophenyl	7.18	WT	8.58	0.080	107.3
		D327G	0.030	0.083	0.361
2-nitrophenyl	7.22	WT	13.67	0.143	95.6
		D327G	0.035	0.133	0.263
3-nitrophenyl	8.39	WT	10.50	0.096	109.4
		D327G	0.042	0.140	0.300
4-bromophenyl	9.34	WT	12.58	0.111	113.3
		D327G	0.016	0.104	0.154
β-naphthyl	9.51	WT	6.26	0.039	160.5
		D327G	0.021	0.225	0.093
phenyl	9.99	WT	5.71	0.176	32.4
		D327G	0.027	0.324	0.083
4-*O*-methylphenyl	10.2	WT	6.69	0.048	139.4
		D327G	0.010	0.088	0.114
3,4-dimethylphenyl	10.32	WT	10.39	0.086	120.8
		D327G	0.010	0.089	0.112

the presence of 100 mM NaN_3 were analyzed by TLC, NMR, and MS spectroscopic techniques and revealed the appearance of a new product (R_f = 0.53) distinct from α-D-galactopyranoside (R_f = 0.27) and Gal-PNP (R_f = 0.64). This new product was identified as azide β-D-galactopyranoside ($N_3\beta$Gal*p*): ^{1}H NMR (D_2O, 500 MHz) δ 4.64 (1H, d, $J_{1,2}$ = 8.6 Hz, H1), 3.98 (1H, d, $J_{3,4}$ = 3.38 Hz, H4), 3.79 (1H, dd, $J_{5,6a}$ = 7.4 Hz $J_{6a,6b}$ = 11.6 Hz, H6a), 3.77 (1H, dd, $J_{5,6b}$ = 5.25 Hz, H6b), 3.75 (1H, dd, H5), 3.68 (1H, dd, $J_{2,3}$ = 9.7 Hz, H3), 3.55 (1H, dd, H2); *m/z* 228.0598 $[N_3\beta Gal p + Na]^+$ (calcd 228.0596).

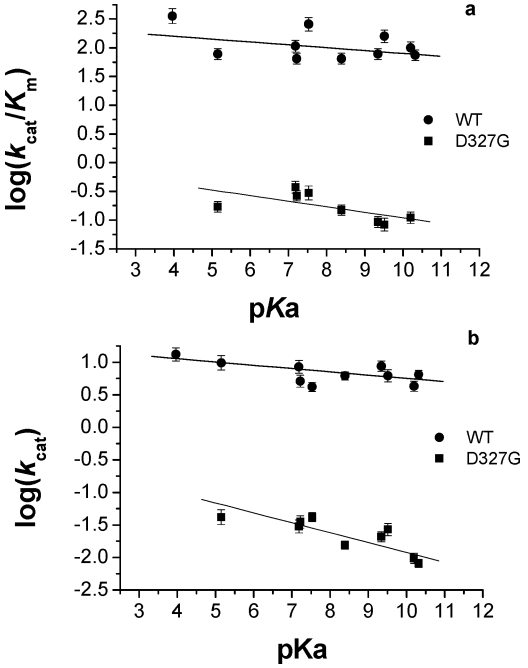

FIGURE 9: Brønsted plots of WT and D327G *Tm*GalA enzymes for aryl galactosides. (a) Effect of leaving group on k_{cat}/K_m: β_{lg} = −0.05 (WT) and β_{lg} = −0.11 (D327G). (b) Effect of leaving group on k_{cat}: β_{lg} = −0.05 (WT) and β_{lg} = −0.15 (D327G). Leaving group ability represented as pK_a: 2,4-dinitrophenyl (4.0); 2,5-dinitrophenyl (5.2); 4-nitrophenyl (7.2); 2-nitrophenyl (7.2); 3-nitrophenyl (8.4); 4-bromophenyl (9.3); β-naphthyl (9.5); phenyl (10.0); 4-*O*-methylphenyl (10.2); 3,4-dimethylphenyl (10.3).

During hydrolysis of Gal-PNP by the D387G enzyme in the presence of 100 mM NaN_3 there was a minimal, 40% increase of hydrolysis rate or catalytic efficiency. NMR revealed that an additional associated signal with a chemical shift at δ = 5.55 ppm appeared as well as the expected signals of α- and β-anomers of D-galactose. After 60 min, the concentration of a new product was estimated to be 0.57 mM (57% of all products obtained). The assignment of chemical shifts for this compound showed it to be azide α-D-galactopyranoside ($N_3\alpha$Gal*p*): ^{1}H NMR (D_2O, 500 MHz) δ 5.55 (1H, d, $J_{1,2}$ = 4.63 Hz, H1), 4.05 (1H, ddd, $J_{5,6a}$ = 7.25 Hz, $J_{5,6b}$ = 4.94 Hz, $J_{5,4}$ = 1.31 Hz, H5), 3.99 (1H, dd, $J_{4,3}$ = 3.31 Hz, H4), 3.93 (1H, dd, $J_{2,3}$ = 10.2 Hz, H2), 3.77 (1H, dd, $J_{6a,6b}$ = 11.8 Hz, H6a), 3.74 (1H, dd, H3), 3.74 (1H, dd, H6b).

DISCUSSION

Several common strategies were used to confirm that GH36 *Tm*GalA, like clan-D member GH27 enzymes (*29*), catalyzes hydrolysis through a double-displacement retaining mechanism (*43*), which involves two consecutive steps (glycosylation and deglycosylation) proceeding via two transition states surrounding the formation of a covalently linked glycosyl-enzyme intermediate (*43*, *51*). As a result of nucleophilic substitution in each step, the C1 atom of the sugar ring is inverted twice, resulting in an overall net retention of the initial stereochemistry. Furthermore,

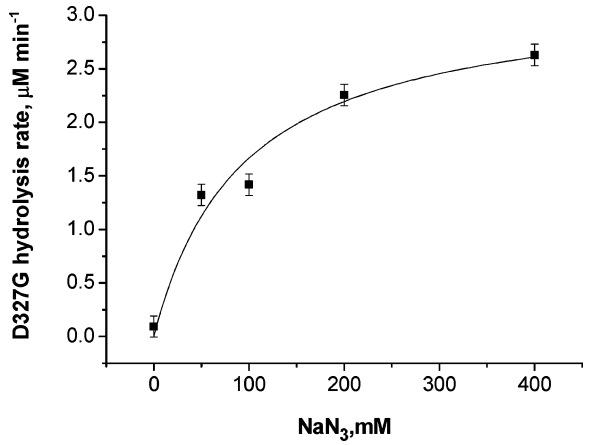

FIGURE 10: Azide rescue of the nucleophile mutant D327G. Reaction conditions: 50 μg of D327G mutant, 50 mM sodium acetate buffer with 0−400 mM sodium azide, and 2.5 mM Gal-PNP, at 37 °C for 20 min.

primary amino acid sequence analysis of GH36 enzymes with respect to those in GH27 revealed a number of conserved acidic amino acid residues. The mutant versions of *Tm*GalA, D327G and D387G, were shown to have less than 1% residual activity on Gal-PNP, consistent with recent reports that residues corresponding to D327 and D387 were the nucleophile and acid/base residues on the α-galactosidase from the hyperthermophile *Sulfolobus solfataricus* (*52*).

Crystallographic data available for glycoside hydrolase clan D have only been available for GH27 enzymes from *H. sapiens*, *G. gallus*, *O. sativa*, and *H. jecorina*. These data have been used to investigate the structural features of lysosomal storage disorders, such as Fabry and Schindler diseases, and show highly conserved catalytic pockets within GH27 (*45*). Structural alignment of *Tm*GalA (1ZY9) confirmed the structural and catalytic similarities between GH27 and GH36 (Figures 2 and 5). Superposition of the *Tm*GalA catalytic pocket with *O. sativa* α-galactosidase indicated that the *Tm*GalA nucleophile is D327 and the acid/base catalyst is D387, based on alignment with *O. sativa* residues D130 and D185, respectively, as shown in Figure 7. This result points to the shared common ancestry of GH27 and GH36 families (*23*). In GH36, catalytic residues are separated by approximately 6.3 Å, rather than the 5.5 Å generally found for retaining enzymes (*30*), which is consistent with an average separation for GH27 catalytic residues of 6.5 Å (*45*). As indicated by structural alignment, the N-terminal domain of *Tm*GalA (residues 1−179) has no homologous structure in GH27 enzymes (Figure 5). This domain, which is found in longer variants in a number of other GH36 α-galactosidases, makes an important contribution to the enzyme active site located within the $(\beta/\alpha)_8$ barrel by providing the key substrate-binding residue W65. Deletion of this domain would likely produce an incorrectly folded and nonfunctional enzyme variant.

To further support the structure-based identification of the catalytic residues, kinetic parameters of the D327G and D387G mutants were compared to those of the WT enzyme. Brønsted analysis of k_{cat} and k_{cat}/K_m values for the hydrolysis of a series of aryl α-galactosides by the WT and D327G enzymes was also performed to obtain information regarding the rate-determining step of catalysis. In the canonical retaining glycoside hydrolase mechanism, the leaving group (aglycon or saccharide) is released during the first step of the reaction with concomitant formation of a covalent glycosyl-enzyme intermediate (enzyme glycosylation). This intermediate is subsequently decomposed by reaction with an exogenous nucleophile, resulting in formation of free enzyme and product by glycosyl transfer (enzyme deglycosylation) (*43*, *51*). Kinetic constants which define the minimal mechanism shown in eq 2 are as follows: $k_{cat} = k_2k_3/(k_2 + k_3)$, $K_m = (k_{-1} + k_2)k_3/(k_2 + k_3)k_1$, and $k_{cat}/K_m = k_1k_2/(k_{-1} + k_2)$, where k_2 and k_3 are the first-order rate constants of the enzyme glycosylation and deglycosylation steps, respectively.

$$E + S \underset{k_{-1}}{\overset{k_1}{\leftrightarrow}} ES \xrightarrow{k_2} E\text{-}S^* \xrightarrow{k_3} E + P_2 \quad (2)$$
$$\downarrow$$
$$P_1$$

Brønsted plots were constructed for WT and D327G *Tm*GalA enzymes (Figure 9) from the kinetic parameters summarized in Table 4. K_m (0.04−0.18 mM) and k_{cat} (5.71−13.67 s^{-1}) values for the WT enzyme did not exhibit large variation across the range of substrates tested. Correspondingly, $\log(k_{cat})$ and $\log(k_{cat}/K_m)$ were essentially independent of the pK_a values of the departing phenol; plots were linear and monotonic with a slope near zero (Figure 9). While the lack of dependence of k_{cat} values on leaving group ability would itself normally be indicative of rate-limiting breakdown of the glycosyl-enzyme intermediate (k_3), the independence of k_{cat}/K_m values on leaving group pK_a precludes this simple conclusion. Regardless of the rate-determining step, the expression $k_{cat}/K_m = (k_1\,k_2)/(k_{-1} + k_2)$ should reflect the first chemical step in the mechanism (governed by k_2, which is necessarily dependent on leaving group ability), except in the case of "sticky" substrates, for which $k_{-1} \ll k_2$. In this case, the expression describing k_{cat}/K_m reduces to $k_{cat}/K_m = k_1$, the rate constant for the association of enzyme and substrate. Observed values of k_{cat}/K_m would therefore be expected to approach the diffusion-controlled reaction rate limit of 10^9−10^{11} M^{-1} s^{-1} (*53*). However, k_{cat}/K_m values are ca. 10^5 for all aryl α-galactosides examined over a pK_a range of 6, so catalysis is unlikely to be limited by the encounter frequency of the enzyme and substrate. A lack of dependence

Table 5: Kinetics of *Tm*GalA WT and Acid−Base Mutant in the Presence of External Nucleophiles

aglycon	pK_a	enzyme	k_{cat} (s^{-1})	ratio k_{cat} (WT/D387G)	K_m (mM)	k_{cat}/K_m (mM^{-1} s^{-1})	ratio k_{cat}/K_m (WT/D387G)
4-nitrophenyl	7.18	WT	33	1500	0.052	620	1000
		D387G	0.022		0.036	0.61	
4-nitrophenyl + azide	7.18	WT	38	1400	0.077	490	1400
		D387G	0.027		0.074	0.36	
4-nitrophenyl + formate	7.18	WT	31	1000	0.044	700	910
		D387G	0.031		0.040	0.77	

of k_{cat}/K_m on pK_a is atypical for retaining glycosidases (*54*−*58*) but is nonetheless precedented. Through detailed kinetic analysis of the hydrolyses of aryl glucosides and glucosyl pyridinium ions by yeast α-glucosidase, together with primary and secondary kinetic isotope measurements, Hosie and Sinnott attributed the insensitivity of kinetic parameters on leaving group phenol pK_a to the existence of a rate-limiting noncovalent step preceding the first bond cleavage event (*59*). On the basis of considerations of the conformational itinerary of the sugar ring during the course of the reaction, it was proposed that the rate-limiting step in this case involved a change from the ground state $^4C_1$ chair conformation of the substrate to a $^{2,5}B$ boat. Although it is tempting to speculate that a similar effect may occur in the *Tm*GalA, which shares identical reaction stereochemistry, much more extensive kinetic analysis would be necessary to test this hypothesis. The family membership of the yeast α-glucosidase studied by Hosie and Sinnott is not known with certainty; however, it is clearly not closely related to *Tm*GalA as genome sequencing of *Saccharomyces cerevisiae* S288C has revealed no GH36 or GH27 sequences (http://afmb.cnrs-mrs.fr/CAZY/geno/4932.html). Therefore, direct mechanistic inferences can, unfortunately, not be drawn between the two enzymes.

Removal of the nucleophilic residue led to a decrease of only 2 orders of magnitude in the rate of hydrolysis of aryl α-galactosides and 3 orders for the catalytic efficiency in comparison with the WT enzyme. The decreased rate and efficiency was independent of the substrate leaving group (Figure 9). This decrease was less than expected for the catalytic efficiency (k_{cat}/K_m) for the nucleophilic mutant (D327G) compared with WT *Tm*GalA (in contrast to more common 10^5-10^8 decrease in k_{cat}/K_m values after mutation) (*60*, *61*). To exclude contamination during purification procedures, new resin was used for each chromatography step for each of the WT and mutant enzymes. Another possible explanation might be a mistranslation of the mRNA codon in the *E. coli* host cell. Smaller decreases (10^4-10^5) have been reported for nucleophilic mutants of other α-glycosidases: *Bacillus circulans* cyclodextrin glycosyltransferase (*62*), α-L-fucosidase from *T. maritima* (*60*), and α-L-arabinofuranosidase from *G. stearothermophilis* (*54*). In the mutation of the α-L-arabinofurnosidase, the double-nucleotide substitution for the targeted amino acid was shown to have a greater difference between WT and nucleophilic enzyme catalytic efficiencies than single-nucleotide substitutions (*54*). A single-nucleotide substitution was used to generate the D327G mutant. While the D327G mutation led to a decrease in activity, additional experiments prove that D327 is the nucleophilic residue.

Values of k_{cat}/K_m and k_{cat} were measured at different pH values. Dependence of both parameters on pH produced bell-shaped curves for the WT and D327G mutant. For the WT, this curve reflects the ionization of the free enzyme and the free substrate (k_{cat}/K_m vs pH) and the enzyme/substrate complex (k_{cat} vs pH). In the case of k_{cat}, these curves illustrate the pH dependence of the rate-limiting step. For the hydrolysis of Gal-PNP (pK_a 7.2) by WT this rate-limiting step is deglycosylation (Figure 9). Mutating the nucleophile (D327G) may result in a concomitant change in the ionization state of the whole catalytic pocket, causing the shift in pH optimum. The pH dependence of catalytic efficiency (k_{cat}/K_m) changed more drastically and may be explained by the decrease in substrate affinity at low pH due to mutation. In the case of D387G, the activity does not decrease at increasing pH. In this case, the pK_a of the remaining catalytic residue was raised, and the nucleophilic residue is deprotonated more effectively at higher pH; hence the reaction rate increases (*63*, *64*). This characteristic response for an acid/base mutant enzyme is observed for *Tm*GalA D387G (Figure 8).

The external nucleophile rescue methodology can provide unambiguous evidence for identification of the putative catalytic residues and the proposed two-step mechanism of catalysis. First is a restoration of the mutant activity in the presence of a small anion, like azide, which occupies cavities in the mutated glycosidase active site. Second is an appearance of a glycosyl azide with inverted (in the case of the nucleophile mutant) or initial (for the acid/base mutant) anomeric configuration. Detection of corresponding products in the reaction mixtures would confirm assignment of the two catalytic residues. Rescue of D327G with azide produced a 30-fold increased hydrolysis rate compared to D327G without azide. The rate clearly depended on the exogenous nucleophile concentration (Figure 10). It was shown that even a small concentration of azide (40 mM) restored the activity of this mutant up to 10-fold, representing a typical behavior for nucleophile mutants of retaining glycosidases (*60*, *65*). Moreover, we have identified by ^1H NMR and mass spectrometry that a new product, $N_3\beta$Gal*p*, appeared in the reaction. Obviously, azide reactivates the D327G mutant through a single inverting displacement to give the β-galactosyl azide product, conclusively proving that D327 is the catalytic nucleophile.

Restoration of activity using external nucleophiles (azide and formate) was attempted on both WT and D387G. The WT did not show any increase in activity in the presence of these nucleophiles, with Gal-PNP as substrate. This is consistent with data on the *S. solfataricus* α-galactosidase, where there was no restoration of activity by azide (*52*). The effect of azide, an exogenous nucleophile, on the hydrolysis of Gal-PNP for the D387G mutant was analyzed by ^1H NMR. A small concentration of azide (100 mM) led to only a 40% increase of mutant hydrolytic activity. However, a new product with α-configuration, $N_3\alpha$Gal*p*, was observed, which should have been formed only at the deglycosylation stage of the process. Formation of $N_3\alpha$Gal*p* in the case of D387G mediated the reaction, and the absence of such a result with the WT is likely due to weakening of the base catalyst in the D387G mutant, suggesting that D387 is an acid/base catalytic amino acid residue. Overall net retention of the anomeric configuration of the C1 atom of the substrate was observed by NMR analysis of products of D387G-catalyzed hydrolysis of Gal-PNP.

These data, combining the pH effect, azide rescue and product characterization, and structural alignment and analysis, conclusively indicate that D327 is the nucleophile and D387 is the acid/base catalytic residues in *Tm*GalA. Addition of sodium azide to the reactions catalyzed by both mutants resulted in restoration of the enzyme activity and formation of new products, $N_3\beta$Gal*p* in case of D327G and $N_3\alpha$Gal*p* in case of D387G. This provides substantial evidence for the double-displacement mechanism of reaction catalyzed by the *Tm*GalA. This study clearly highlights the common

active site structure and catalytic mechanism shared between GH27 and GH36 enzymes in clan GH-D. It is anticipated that this contribution to understanding protein structure-function relationships in this clan will serve to direct future efforts focusing on catalytically engineering these enzymes for biotechnological purposes.

SUPPORTING INFORMATION AVAILABLE

^{1}H NMR analysis for the substituted α-D-galactopyranosides. This material is available free of charge via the Internet at http://pubs.acs.org.

REFERENCES

1. Meier, H., and Reid, J. S. G. (1982) Reserve polysaccharides other than starch in higher plants, in *Encyclopedia of Plant Physiology* (Loewus, F. A., and Tanner, W., Eds.) pp 418−471, Springer-Verlag, New York.
2. Eng, C. M., Guffon, N., Wilcox, W. R., Germain, D. P., Lee, P., Waldek, S., Caplan, L., Linthorst, G. E., and Desnick, R. J. (2001) Safety and efficacy of recombinant human alpha-galactosidase a replacement therapy in Fabry's disease, *N. Engl. J. Med. 345*, 9−16.
3. Gieselmann, V. (1995) Lysosomal storage diseases, *Biochim. Biophys. Acta 1270*, 103−136.
4. Sakuraba, H., Matsuzawa, F., Aikawa, S., Doi, H., Kotani, M., Nakada, H., Fukushige, T., and Kanzaki, T. (2004) Structural and immunocytochemical studies on alpha-N-acetylgalactosaminidase deficiency (Schindler/Kanzaki disease), *J. Hum. Genet. 49*, 1−8.
5. Ghazi, S., Rooke, J. A., and Galbraith, H. (2003) Improvement of the nutritive value of soybean meal by protease and alpha-galactosidase treatment in broiler cockerels and broiler chicks, *Br. Poult. Sci. 44*, 410−418.
6. Ganter, C., Bock, A., Buckel, P., and Mattes, R. (1988) Production of thermostable, recombinant alpha-galactosidase suitable for raffinose elimination from sugar-beet syrup, *J. Biotechnol. 8*, 301−310.
7. Thananunkul, D., Tanaka, M., Chichester, C. O., and Lee, T. C. (1976) Degradation of raffinose and stachyose in soybean milk by alpha-galactosidase from *Mortierella vinacea*−Entrapment of alpha-galactosidase within polyacrylamide-gel, *J. Food Sci. 41*, 173−175.
8. Dey, P. M., Patel, S., and Brownleader, M. D. (1993) Induction of alpha-galactosidase in *Penicillium ochrochloron* by guar (*Cyamopsis tetragonobola*) gum, *Biotechnol. Appl. Biochem. 17*, 361−371.
9. Tayal, A., Pai, V. B., and Khan, S. A. (1999) Rheology and microstructural changes during enzymatic degradation of a guar-borax hydrogel, *Macromolecules 32*, 5567−5574.
10. McCutchen, C. M., Duffaud, G. D., Leduc, P., Petersen, A. R. H., Tayal, A., Khan, S. A., and Kelly, R. M. (1996) Characterization of extremely thermostable enzymatic breakers (alpha-1,6-galactosidase and beta-1,4-mannanase) from the hyperthermophilic bacterium *Thermotoga neapolitana* 5068 for hydrolysis of guar gum, *Biotechnol. Bioeng. 52*, 332−339.
11. Goldstein, J., Siviglia, G., Hurst, R., Lenny, L., and Reich, L. (1982) Group-B erythrocytes enzymatically converted to group-O survive normally in A, B, and O individuals, *Science 215*, 168−170.
12. Lenny, L. L., Hurst, R., Goldstein, J., and Galbraith, R. A. (1994) Transfusions to group-O subjects of 2 units of red-cells enzymatically converted from group-B to group-O, *Transfusion 34*, 209−214.
13. Kruskall, M. S., AuBuchon, J. P., Anthony, K. Y., Herschel, L., Pickard, C., Biehl, R., Horowitz, M., Brambilla, D. J., and Popovsky, M. A. (2000) Transfusion to blood group A and O patients of group B RBCs that have been enzymatically converted to group O, *Transfusion 40*, 1290−1298.
14. Hata, D. J., and Smith, D. S. (2004) Blood group B degrading activity of *Ruminococcus gnavus* alpha-galactosidase, *Artif. Cells, Blood Substitutes, Biotechnol. 32*, 263−274.
15. Dean, K. J., and Sweeley, C. C. (1979) Studies on human-liver alpha-galactosidases. 1. Purification of alpha-galactosidase-A and its enzymatic properties with glycolipid and oligosaccharide substrates, *J. Biol. Chem. 254*, 9994.
16. Dean, K. J., and Sweeley, C. C. (1979) Studies on human-liver alpha-galactosidases. 2. Purification and enzymatic properties of alpha-galactosidase B (alpha-N-acetylgalactosaminidase), *J. Biol. Chem. 254*, 1−5.
17. Ademark, P., de Vries, R. P., Hagglund, P., Stalbrand, H., and Visser, J. (2001) Cloning and characterization of *Aspergillus niger* genes encoding an alpha-galactosidase and a beta-mannosidase involved in galactomannan degradation, *Eur. J. Biochem. 268*, 2982−2990.
18. Liebl, W., Wagner, B., and Schellhase, J. (1998) Properties of an alpha-galactosidase, and structure of its gene galA, within an alpha- and beta-galactoside utilization gene cluster of the hyperthermophilic bacterium *Thermotoga maritima*, *Syst. Appl. Microbiol. 21*, 1−11.
19. Dey, P. M., Delcampillo, E. M., and Lezica, R. P. (1983) Characterization of a glycoprotein alpha-galactosidase from lentil seeds (*Lens culinaris*), *J. Biol. Chem. 258*, 923−929.
20. Henrissat, B., and Bairoch, A. (1996) Updating the sequence-based classification of glycosyl hydrolases, *Biochem. J. 316*, 695−696.
21. Henrissat, B. (1991) A classification of glycosyl hydrolases based on amino-acid-sequence similarities, *Biochem. J. 280*, 309−316.
22. Henrissat, B., and Bairoch, A. (1993) New families in the classification of glycosyl hydrolases based on amino-acid-sequence similarities, *Biochem. J. 293*, 781−788.
23. Rigden, D. J. (2002) Iterative database searches demonstrate that glycoside hydrolase families 27, 31, 36 and 66 share a common evolutionary origin with family 13, *FEBS Lett. 523*, 17−22.
24. Garman, S. C., Hannick, L., Zhu, A., and Garboczi, D. N. (2002) The 1.9 Ångström structure of alpha-N-acetylgalactosaminidase: Molecular basis of glycosidase deficiency diseases, *Structure 10*, 425−434.
25. Garman, S. C., and Garboczi, D. N. (2004) The molecular defect leading to Fabry disease: Structure of human alpha-galactosidase, *J. Mol. Biol. 337*, 319−335.
26. Golubev, A. M., Nagem, R. A. P., Neto, J. R. B., Neustroev, K. N., Eneyskaya, E. V., Kulminskaya, A. A., Shabalin, K. A., Savel'ev, A. N., and Polikarpov, I. (2004) Crystal structure of alpha-galactosidase from *Trichoderma reesei* and its complex with galactose: Implications for catalytic mechanism, *J. Mol. Biol. 339*, 413−422.
27. Kuhls, K., Lieckfeldt, E., Samuels, G. J., Kovacs, W., Meyer, W., Petrini, O., Gams, W., Borner, T., and Kubicek, C. P. (1996) Molecular evidence that the asexual industrial fungus *Trichoderma reesei* is a clonal derivative of the ascomycete *Hypocrea jecorina*, *Proc. Natl. Acad. Sci. U.S.A. 93*, 7755−7760.
28. Fujimoto, Z., Kaneko, S., Momma, M., Kobayashi, H., and Mizuno, H. (2003) Crystal structure of rice alpha-galactosidase complexed with D-galactose, *J. Biol. Chem. 278*, 20313−20318.
29. Brumer, H., Sims, P. F. G., and Sinnott, M. L. (1999) Lignocellulose degradation by *Phanerochaete chrysosporium*: purification and characterization of the main alpha-galactosidase, *Biochem. J. 339*, 43−53.
30. Rye, C. S., and Withers, S. G. (2000) Glycosidase mechanisms, *Curr. Opin. Chem. Biol. 4*, 573−580.
31. Hart, D. O., He, S. M., Chany, C. J., Withers, S. G., Sims, P. F. G., Sinnott, M. L., and Brumer, H. (2000) Identification of Asp-130 as the catalytic nucleophile in the main alpha-galactosidase from *Phanerochaete chrysosporium*, a family 27 glycosyl hydrolase, *Biochemistry 39*, 9826−9836.
32. Ly, H. D., Howard, S., Shum, K., He, S. M., Zhu, A., and Withers, S. G. (2000) The synthesis, testing and use of 5-fluoro-alpha-D-galactosyl fluoride to trap an intermediate on green coffee bean alpha-galactosidase and identify the catalytic nucleophile, *Carbohyd. Res. 329*, 539−547.
33. Garman, S. C., and Garboczi, D. N. (2002) Structural basis of Fabry disease, *Mol. Genet. Metab. 77*, 3−11.
34. Lesley, S. A., Kuhn, P., Godzik, A., Deacon, A. M., Mathews, I., Kreusch, A., Spraggon, G., Klock, H. E., McMullan, D., Shin, T., Vincent, J., Robb, A., Brinen, L. S., Miller, M. D., McPhillips, T. M., Miller, M. A., Scheibe, D., Canaves, J. M., Guda, C., Jaroszewski, L., Selby, T. L., Elsliger, M. A., Wooley, J., Taylor, S. S., Hodgson, K. O., Wilson, I. A., Schultz, P. G., and Stevens, R. C. (2002) Structural genomics of the *Thermotoga maritima* proteome implemented in a high-throughput structure determination pipeline, *Proc. Natl. Acad. Sci. U.S.A. 99*, 11664−11669.
35. Montgomery, E. M., Richtmyer, N. K., and Hudson, C. S. (1942) The preparation and rearrangement of phenylglycosides, *J. Am. Chem. Soc. 64*, 690−694.

36. Ibatullin, F. M., and Selivanov, S. I. (2002) Reaction of 1,2-trans-glycosyl acetates with phosphorus pentachloride: new efficient approach to 1,2-trans-glycosyl chlorides, *Tetrahedron Lett. 43*, 9577−9580.
37. Delmotte, F. M., Privat, J., and Monsigny, M. L. P. (1975) Glycan-protein interactions—Synthesis of 4-methylumbelliferyl-2-acetamido-2-deoxy-beta-D-glucopyranoside, 4-methylumbelliferyl-di-N-acetyl-beta-chitobioside and 4-methyl-tri-N-acetyl-beta-chitotrioside—Interaction of these osides with lysozyme, *Carbohydr. Res. 40*, 353−364.
38. Apparu, M., Blancmuesser, M., Defaye, J., and Driguez, H. (1981) Stereoselective syntheses of *O*-nitrophenyl and *S*-nitrophenyl glycosides. 3. Syntheses in the alpha-D-galactopyranose and alpha-maltose series, *Can. J. Chem. 59*, 314−320.
39. Miller, E. S., Parker, K. N., Liebl, W., Lam, D., Callen, W., Snead, M. A., Mathur, E. J., Short, J. M., and Kelly, R. M. (2001) alpha-D-galactosidases from *Thermotoga* species, *Methods Enzymol. 330*, 246−260.
40. Eneyskaya, E. V., Ivanen, D. R., Shabalin, K. A., Kulminskaya, A. A., Backinowsky, L. V., Brumer, H., Neustroev, K. N. (2005) Chemo-enzymatic synthesis of 4-methylumbelliferyl beta-(1→4)-D-xylooligosides: new substrates for beta-D-xylanase assays, *Org. Biomol. Chem. 3*, 146−151.
41. Davies, G. J., Wilson, K. S., and Henrissat, B. (1997) Nomenclature for sugar-binding subsites in glycosyl hydrolases, *Biochem. J. 321*, 557−559.
42. Thompson, J. D., Higgins, D. G., and Gibson, T. J. (1994) ClustalW—Improving the sensitivity of progressive multiple sequence alignment through sequence weighting, position-specific gap penalties and weight matrix choice, *Nucleic Acids Res. 22*, 4673−4680.
43. Sinnott, M. L. (1990) Catalytic mechanisms of enzymatic glycosyl transfer, *Chem. Rev. 90*, 1171−1202.
44. Holm, L., and Park, J. (2000) DaliLite workbench for protein structure comparison, *Bioinformatics 16*, 566−567.
45. Garman, S. C. (2006) Structural studies on alpha-GAL and alpha-NAGAL: The atomic basis of Fabry and Schindler diseases, *Biocatal. Biotransform. 24*, 129−136.
46. Heikinheimo, P., Helland, R., Leiros, H. K. S., Leiros, I., Karlsen, S., Evjen, G., Ravelli, R., Schoehn, G., Ruigrok, R., Tollersrud, O. K., McSweeney, S., and Hough, E. (2003) The structure of bovine lysosomal alpha-mannosidase suggests a novel mechanism for low-pH activation, *J. Mol. Biol. 327*, 631−644.
47. Holm, L., and Sander, C. (1993) Protein-structure comparison by alignment of distance matrices, *J. Mol. Biol. 233*, 123−138.
48. Krissinel, E., and Henrick, K. (2004) Secondary-structure matching (SSM), a new tool for fast protein structure alignment in three dimensions, *Acta Crystallogr. D 60*, 2256−2268.
49. Bravman, T., Mechaly, A., Shulami, S., Belakhov, V., Baasov, T., Shoham, G., and Shoham, Y. (2001) Glutamic acid 160 is the acid-base catalyst of beta-xylosidase from *Bacillus stearothermophilus* T-6: a family 39 glycoside hydrolase, *FEBS Lett. 495*, 115−119.
50. Shallom, D., Belakhov, V., Solomon, D., Gilead-Gropper, S., Baasov, T., Shoham, G., and Shoham, Y. (2002) The identification of the acid-base catalyst of alpha-arabinofuranosidase from *Geobacillus stearothermophilus* T-6, a family 51 glycoside hydrolase, *FEBS Lett. 514*, 163−167.
51. Vocadlo, D. J., Davies, G. J., Laine, R., and Withers, S. G. (2001) Catalysis by hen egg-white lysozyme proceeds via a covalent intermediate, *Nature 412*, 835−838.
52. Brouns, J. J. S., Smits, N., Wu, H., Snijders, A. P. L., Wright, P. C., de Vos, W. M., and van der Oost, J. (2006) Identification of a novel alpha-galactosidase from the hyperthermophilic archaeon *Sulfolobus solfataricus*, *J. Bacteriol. 188*, 2392−2399.
53. Fersht, A. (1985) *Enzyme Structure and Mechanism*, 2nd ed., Vol. 2, W. H. Freeman, San Francisco, CA.
54. Shallom, D., Belakhov, V., Solomon, D., Shoham, G., Baasov, T., and Shoham, Y. (2002) Detailed kinetic analysis and identification of the nucleophile in alpha-L-arabinofuranosidase from *Geobacillus stearothermophilus* T-6, a family 51 glycoside hydrolase, *J. Biol. Chem. 277*, 43667−43673.
55. Bauer, M. W., and Kelly, R. M. (1998) The family 1 beta-glucosidases from *Pyrococcus furiosus* and *Agrobacterium faecalis* share a common catalytic mechanism, *Biochemistry 37*, 17170−17178.
56. Kempton, J. B., and Withers, S. G. (1992) Mechanism of *Agrobacterium* beta-glucosidase—Kinetic studies, *Biochemistry 31*, 9961−9969.
57. Malet, C., and Planas, A. (1997) Mechanism of *Bacillus* 1,3−1,4-beta-D-glucan 4-glucanohydrolases: Kinetics and pH studies with 4-methylumbelliferyl beta-D-glucan oligosaccharides, *Biochemistry 36*, 13838−13848.
58. Namchuk, M., Braun, C., McCarter, J. D., and Withers, S. G. (1996) Fluorinated sugars as probes of glycosidase mechanisms, *ACS Symp. Ser.*, 279−293.
59. Hosie, L., and Sinnott, M. L. (1985) Effects of deuterium substitution alpha and beta to the reaction centre, ^{18}O substitution in the leaving group, and aglycone acidity on hydrolyses of aryl glucosides and glucosyl pyridinium ions by yeast alpha-glucosidase. A probable failure of the antiperiplanar-lone-pair hypothesis in glycosidase catalysis, *Biochem. J. 226*, 437−446.
60. Tarling, C. A., He, S. M., Sulzenbacher, G., Bignon, C., Bourne, Y., Henrissat, B., and Withers, S. G. (2003) Identification of the catalytic nucleophile of the family 29 alpha-L-fucosidase from *Thermotoga maritima* through trapping of a covalent glycosyl-enzyme intermediate and mutagenesis, *J. Biol. Chem. 278*, 47394−47399.
61. Viladot, J. L., de Ramon, E., Durany, O., and Planas, A. (1998) Probing the mechanism of *Bacillus* 1,3−1, 4-beta-D-glucan 4-glucanohydrolases by chemical rescue of inactive mutants at catalytically essential residues, *Biochemistry 37*, 11332−11342.
62. Knegtel, R. M., Strokopytov, B., Penninga, D., Faber, O. G., Rozeboom, H. J., Kalk, K. H., Dijkhuizen, L., and Dijkstra, B. W. (1995) Crystallographic studies of the interaction of cyclodextrin glycosyltransferase from *Bacillus circulans* strain 251 with natural substrates and products, *J. Biol. Chem. 270*, 29256−29264.
63. Bravman, T., Belakhov, V., Solomon, D., Shoham, G., Henrissat, B., Baasov, T., and Shoham, Y. (2003) Identification of the catalytic residues in family 52 glycoside hydrolase, a beta-xylosidase from *Geobacillus stearothermophilus* T-6, *J. Biol. Chem. 278*, 26742−26749.
64. Li, Y. K., Chir, J., Tanaka, S., and Chen, F. Y. (2002) Identification of the general acid/base catalyst of a family 3 beta-glucosidase from *Flavobacterium meningosepticum*, *Biochemistry 41*, 2751−2759.
65. Viladot, J. L., de Ramon, E., Durany, O., and Planas, A. (1998) Probing the mechanism of *Bacillus* 1,3−1,4-beta-D-glucan 4-glucanohydrolases by chemical rescue of inactive mutants at catalytically essential residues, *Biochemistry 37*, 11332−11342.

BI061521N